

## Electric-dipole spin-resonance study on extended defects in Czochralski-grown silicon developed by thermal treatment

T. R. Mchedlidze,\* V. V. Kveder,\* J. Jablonski,<sup>†</sup> and K. Sumino  
*Institute for Material Research, Tohoku University, Sendai 980, Japan*

(Received 22 November 1993)

A series of electric-dipole spin-resonance (EDSR) lines, termed Si-SC1 lines, are found to develop in Czochralski-grown Si crystals due to annealing at 650°C. Some of these lines are very close to Si-2K and Si-3K reported in a previous work. The experimental data are self-consistently explained by use of a model that shows that the EDSR signals are caused by additional electrons trapped by long quasi-one-dimensional defects lying along the  $\langle 110 \rangle$  directions. The localization length of the trapped electrons is determined to be of the order of 100 nm and their mobility to be rather high along the defects, suggesting that a quasi-one-dimensional energy band is associated with the straight part of the defect. Si-SC1 centers are attributed to the so-called rodlike defects that are developed in the Czochralski-grown Si crystals due to the above heat treatment.

### I. INTRODUCTION

Investigation of defects induced in Czochralski-grown Si crystals (CZ-Si) due to heat treatment in the temperature range 600–800°C is of great interest because such heat treatment is often involved in device fabrication processes. Observations with transmission electron microscopy (TEM) have revealed that several different kinds of extended defects are present in CZ-Si after such heat treatment: They are oxide precipitates of a plate shape (PLP's), rodlike (or ribbonlike) defects (RLD's), and elongated dislocation dipoles (DD's).<sup>1–7</sup> The electronic properties of these extended defects are far from understood. It is known from measurements of the Hall effect and deep level transient spectroscopy (DLTS) that a number of donor states [termed new donors (ND)] appear in CZ-Si after such heat treatment.<sup>8,9</sup> It is reported that there is a strong correlation between the intensity of one of the DLTS peaks, termed ND2, and the concentration of RLD's in phosphorus-doped and carbon-lean CZ-Si, which is preannealed at 450°C and subsequently annealed at 650°C.<sup>10</sup> However, even if ND2 is correlated with RLD's, it is by no means clear whether such a donor state is an attribute of a straight part of RLD or that of some geometrical irregularities discretely distributed along the RLD.

A very powerful experimental method for investigating the electronic properties of extended defects is electric-dipole spin resonance (EDSR), which has already been successfully used for the investigation of the electronic state associated with dislocations in plastically deformed floating-zone-grown Si.<sup>11,12</sup> The EDSR signal from thermally treated CZ-Si was reported by Babich and co-workers<sup>13,14</sup> and was attributed to DD's.

EDSR results from the coupling between electron momentum  $\mathbf{p}$  and its spin  $\mathbf{S}$  caused by spin-orbital interaction. In the absence of inversion symmetry this interaction leads to the appearance of the term  $[\mathbf{V} \times \mathbf{p}] \cdot \mathbf{S}$  in the electron Hamiltonian,<sup>15</sup> where  $\mathbf{V}$  is some vector having the dimension of velocity. It means that the electron spin is affected by effective magnetic field

$\mathbf{h} = [\mathbf{V} \times \mathbf{p}] / g\mu_B$ , where  $g$  and  $\mu_B$  are the  $g$  factor and the Bohr magneton, respectively. Application of the external electric field  $\mathbf{E}_\omega$  with a frequency  $\omega$  induces the momentum component with the same frequency  $\mathbf{p}_\omega = \eta \mathbf{E}_\omega$ , where  $\eta$  is a complex tensor which characterizes the polarizability of the electron system. Under a magnetic field, the magnitude of which is equal to  $H_0 = \hbar\omega / g\mu_B$ , the effective field  $\mathbf{h}_\omega = [\mathbf{V} \times \mathbf{p}_\omega] / g\mu_B$  excites transitions between the Zeeman levels and results in a strong resonance singularity of the dielectric permeability  $\epsilon(\omega) = \epsilon' + i\epsilon''$  of the sample, which is called EDSR.

The EDSR intensity is proportional to  $(\mathbf{V} \eta \mathbf{E}_\omega)^2$ . Due to the symmetry of a crystal,  $\mathbf{V}$  is zero for free electrons in Si.<sup>15</sup> However, if an electron is localized on a defect having no inversion symmetry and the extension  $R$  of the electronic wave function is small along the direction in which the inversion symmetry is lost, the magnitude of  $V$  ( $\equiv |\mathbf{V}|$ ) can be rather large. On the other hand,  $\eta$  can be large only if the extension  $L$  of the electronic wave function is large along the direction of  $\mathbf{E}_\omega$ . In such a case  $\eta$  is proportional to  $L^4$  for  $L < 40$  nm and  $\omega = 6 \times 10^{10} \text{ sec}^{-1}$ . For these reasons, the EDSR in Si becomes observable for electrons trapped by some extended defects with low symmetry. Contrarily, the EDSR intensity is small for electrons trapped by point defects where  $L$  is comparable to  $R$ . It is smaller than or comparable to the intensity of usual electron paramagnetic resonance (EPR) for both deep and shallow point defects at the X-band frequency of  $\omega = 6 \times 10^{10} \text{ s}^{-1}$ .

Contrary to the case of point defects, we can expect very strong EDSR for regular parts of one- or two-dimensional extended defects, provided that such defects no longer maintain inversion symmetry in the direction perpendicular to themselves and that they accompany deep electronic states within the band gap. The magnitude of  $V$  at such a defect can be high enough since an electron is strongly localized in the direction perpendicular to the defect and the magnitude of  $\eta$  can be high since the localization length of an electron is large enough along the defect ( $L \gg R$ ).

TABLE I. Defect density  $N_D$ , EDSR absorption intensity  $A$ , and concentration of free electrons at 300 K  $n_{300}$  in samples. Samples 1 and 2 are doped with phosphorus and samples 3–6 are doped with boron. Sample 2 has been preannealed at 450°C for 160 h before annealing at 650°C.

Sample	Annealing time at 650°C (h)	$N_D$			$A$ Arbitrary unit	$n_{300}$ ( $\times 10^{14}$ cm $^{-3}$ )
		RLD's ( $\times 10^7$ cm $^{-2}$ )	DD's ( $\times 10^7$ cm $^{-2}$ )	PLP's ( $\times 10^{11}$ cm $^{-3}$ )		
1	160	4.5±1.1	1.1±0.3	5	1.0	9.3
2	160	1.3±0.5	1.5±0.5		2.0	35.0
3	260	1.4±0.6	1.5±0.6	0.2	0.1	5.7
4	160	2.1±0.7	1.0±0.4	0.05	0.25	4.7
5	120	1.5±0.6	0.2±0.1	<0.01	0.13	3.9
6	80	<0.2	<0.2	<0.01	<0.02	3.5

In the case of annealed CZ-Si suitable objects for the EDSR study may be rodlike defects (RLD's), dislocation dipoles (DD's), and platelike precipitates (PLP's), if they accompany electronic states within the forbidden gap. The purpose of this work is to investigate the electronic states of extended defects which develop in thermally treated CZ-Si by means of the EDSR. We mainly concentrate on the temperature dependence of the EDSR and estimate the electron localization length and other related parameters. Such attempts were not done in the previous works.<sup>13,14</sup>

## II. EXPERIMENT

Investigations were done with CZ-Si of both  $n$  and  $p$  type, the carbon concentration of which was lower than the detection limit of the Fourier transform infrared spectroscopy (FTIR), namely, lower than  $2 \times 10^{16}$  cm $^{-3}$ . The  $n$ -type crystal was doped with phosphorus at a concentration of  $1.4 \times 10^{14}$  atoms/cm $^3$  while the  $p$ -type crystal with boron at a concentration of  $4 \times 10^{14}$  atoms/cm $^3$ . The concentrations of interstitial oxygen atoms determined by means of FTIR were  $1.0 \times 10^{18}$  atoms/cm $^3$  in the  $n$ -type crystal and  $8.7 \times 10^{17}$  atoms/cm $^3$  in the  $p$ -type crystal with a conversion factor of the Japan Industry Development Association (JEIDA).<sup>16</sup> Samples with a dimension of  $5 \times 5 \times 15$  mm $^3$  in size were sealed within evacuated quartz capsules and were annealed at 650°C. Annealing times of the samples are given in Table I.

A JEOL X-band ESR spectrometer was used to measure the spin resonance of samples. A standard cylindrical microwave cavity of the TE (011) mode was used for the measurements of EPR. In this case, the sample was set at the position where the microwave magnetic field  $H_\omega$  was maximum and the microwave electric field  $E_\omega$  was nearly zero. A rectangular cavity of the TE (103) mode specially designed and fabricated was used for EDSR measurements. In this case, the sample was set at the position where  $E_\omega$  was maximum and  $H_\omega$  was negligible. A standard-type Oxford cryostat was used to control sample temperature. The derivative of microwave absorption with respect to magnetic field was measured using a lock-in amplifier and the magnetic field modulation with an amplitude of 0.2 Oe at 100 kHz in the frequency. The signal intensity as well as the  $g$  value was calibrated using the EPR standard (Mn $^{++}$  in MgO) which was set

at the maximum of  $H_\omega$  within the microwave cavity. The EPR standard was kept at room temperature during the measurements.

TEM observations of samples used in EDSR measurements were done with a JEOL JEM-2000EX microscope operating at 200 KV under a two-beam (with diffraction vectors of 220 type) or a multibeam condition. Bright field images were taken with thinned samples parallel to one of the {111} planes. First, the sum of the density of DD's and that of RLD's was determined by counting the intersections of these defects with the surface of the TEM sample. The relative densities of the two kinds of defects were determined from the ratio of the total lengths of the segments of each kind of defects in the thin sample. Disappearance of RLD images with a diffraction vector parallel to themselves was used to distinguish between the RLD's and DD's. The density of PLP's was also determined.

The concentration of uncompensated shallow donors in each sample after annealing was determined by means of four points probe resistivity measurements at room temperature using the standard Irving curves.

## III. EXPERIMENTAL RESULTS

### A. TEM observations and EPR and EDSR spectra

Typical TEM micrographs of samples 1 and 2 are shown in Fig. 1. The three kinds of extended defects, namely, RLD's, DD's, and PLP's, are all seen there. RLD's and DD's are both observed to be elongated along the  $\langle 110 \rangle$  directions. TEM micrographs of samples 3, 4, and 5 are similar to that of sample 1.

Figures 2(a) and 2(b) show typical EPR and EDSR absorption spectra, respectively, obtained with samples 1 and 2 at 10 K. The EPR spectra show an intense and nearly isotropic absorption line with the  $g$  value close to 1.999 besides the phosphorus doublet as demonstrated with sample 1 in Fig. 2(a). This signal is similar to one observed in previous works,<sup>17,18</sup> in which it was related to new donors (ND's). The phases of 100 kHz absorption signals at the input of the lock-in amplifier for both phosphorus and ND lines do not correspond to those of slow passage condition at this temperature. The *in phase* (denoted by 0° in the figure) and *out of phase* (denoted by 90°) EPR signals are both shown in Fig. 2(a). The phase

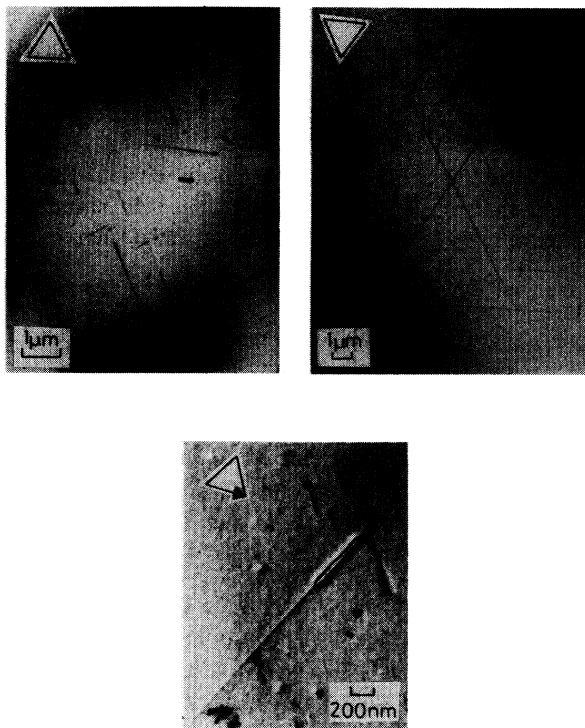


FIG. 1. Transmission electron micrographs of (a) sample 1, (b) sample 2 under the multibeam condition, and (c) sample 1 under the two-beam condition with diffraction vector 220. Triangles shown on the micrographs consist of lines parallel to the  $\langle 110 \rangle$  directions lying on the film plane.

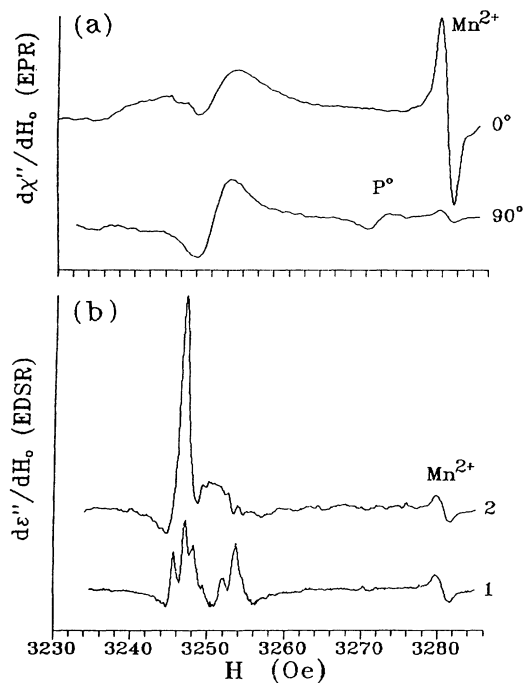


FIG. 2. (a) In-phase (marked  $0^\circ$ ) and out-of-phase (marked  $90^\circ$ ) EPR absorption spectra of sample 1 and (b) EDSR absorption spectra of sample 1 (marked 1) and sample 2 (marked 2) at 10 K.

shifts of EPR related to phosphorus and ND result from rather small spin-lattice relaxation rate  $\tau_1^{-1}$  for these centers; namely, smaller than the modulation frequency 100 kHz used in the experiment.

Instead of ND lines, many narrow lines are detected in EDSR as seen in Fig. 2(b). The intensity of the EDSR signal is much higher than the total EPR signal intensity of ND and phosphorus in the same sample and is not affected by the latter. The phase of the EDSR signal was found to correspond to that of the normal slow passage condition and no *out-of-phase* signal was detected in this case.

### B. Angular dependence of EDSR

As seen in Fig. 2(b), the number and amplitude of EDSR lines depend strongly on the thermal history of the sample. Figures 3(a) and 3(b) show the angular dependencies of the  $g$  factor within the (001) plane for samples 1 and 2, respectively. Filled marks are for strong EDSR lines, whereas open marks are for weak lines which we do not discuss here. All lines are caused by paramagnetic centers with  $S = \frac{1}{2}$  and we assume that the spin Hamiltonian is given by  $\sum \mu_B g_{ij} S_i H_j$ .

Analyzing the angular dependencies of  $g$  factors of the EDSR-active centers for the rotation around the [001] and the [110] axes, we found that one of the principal axes (denoted by L axis, hereafter) is parallel to one of the  $\langle 110 \rangle$  directions, while another one (denoted by Y axis)

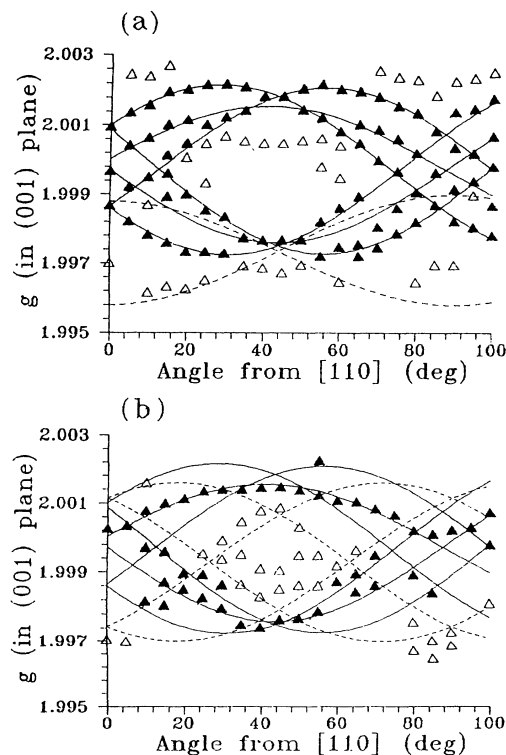


FIG. 3. Angular dependence of the  $g$  factor of EDSR in (a) sample 1 and (b) sample 2 around the rotation axis of the [001].

is different for different centers, but ranging always between the  $\langle 1\bar{1}3 \rangle$  and the  $\langle \bar{1}13 \rangle$  directions perpendicular to  $L$ . Centers with  $L$  parallel to all crystallographically equivalent  $\langle 110 \rangle$  directions are observed to be present at approximately equal concentrations. The  $g_L$  value is determined to be  $1.9958 \pm 0.0003$ . For a given  $L$  axis (for instance,  $L$  parallel to  $[110]$ ) up to three intensive lines are observed. One of them has a  $Y$  axis parallel to  $[001]$  with an accuracy of  $\pm 5^\circ$  and  $g_y \approx 2.0017$  and  $g_z \approx 1.9994$ . Two others have  $Y$  axes close to  $[\bar{1}13]$  or  $[1\bar{1}3]$  with  $g_y \approx 2.0026$  and  $g_z \approx 1.9986$ , the accuracy being  $\pm 3 \times 10^{-4}$ .

In the geometry with  $E_\omega$  parallel to  $H_0$  the amplitude  $A$  of the EDSR lines with a given  $L$  axis is found to be described well with a relation  $A \propto (L \cdot E_\omega)^2$ . It implies that  $\eta$  is much larger along the  $L$  axis than along two other axes, which can be interpreted only with the idea that the electron wave function has a much longer localization length along the  $L$  direction than along other directions. This is a strong indication showing that the observed EDSR signals originate from some linear defects lying along the  $\langle 110 \rangle$  directions.

Data in Figs. 3(a) and 3(b) were obtained with  $E_\omega$  applied parallel to the rotation axis  $[001]$ . Solid curves in the figures were those calculated using the above given parameters of  $g$  tensors for  $L \parallel [101]$  and  $L \parallel [011]$ . Dashed curves are for  $L \parallel [110]$  and  $L \parallel [1\bar{1}0]$ . In the latter case  $L$  is perpendicular to  $E_\omega$ , so that the EDSR lines originating from linear defects lying along such directions should be absent. Indeed, they were observed to be very weak and are thought to be caused by small nonuniformity of  $E_\omega$ . The  $g$  tensors determined for strong EDSR lines are not in accordance with those determined for Si-2K, 3K, and 4K centers in the previous works.<sup>14</sup> However, the  $g$  tensors of some weak EDSR lines were found to coincide well with those determined for such centers.

Parameters such as line width, shape, and their dependencies on temperature or on microwave power are very similar for all the strong EDSR lines observed. This suggests that defects giving rise to these EDSR lines are of the same nature. We term these defects Si-SC1 centers.

All measurements described in the following were made with samples in the orientation corresponding to the angle  $45^\circ$  in Fig. 3 and with  $E_\omega$  parallel to the  $[001]$  direction. Measurements were done with the most intensive line of the spectrum. Each EDSR spectrum was decomposed into individual lines by a computer so as to have the best fit. The shape of the lines used for fitting was calculated with Eq. (6) given in Sec. IV. The EDSR amplitude was divided by the amplitude of EPR signal from the Mn standard and also by the volume of the sample.

### C. Microwave conductivity

In EDSR measurements, a sample is set at the position of the maximum of microwave electric field  $E_\omega$  and the EDSR signal just corresponds to the change in the real part of microwave conductivity of the sample  $\sigma_\omega = \omega \epsilon''(\omega) / 4\pi$  due to spin resonance. The absolute

value of  $\sigma_\omega$  which is out of resonance can also be calculated from the change in  $Q$  factor of the cavity caused by the sample. Taking into account that

$$Q^{-1} = (2\pi V_s \sigma_\omega / \omega V_c) + Q_0^{-1}, \quad (1)$$

where  $Q_0$  is the  $Q$  factor for the cavity without the sample, and that the EPR signal from the Mn standard is proportional to  $Q$ , we can calculate  $\sigma_\omega$  from the relation

$$\sigma_\omega = \alpha (A_e / A_s - 1) / V_s, \quad (2)$$

where  $V_s$  and  $V_c$  are the volumes of the sample and the cavity, respectively, and  $A_s$  and  $A_e$  are the intensities of the EPR-standard signal for the cavity with and without the sample, respectively. Though the coefficient  $\alpha$  could be easily estimated, we preferred to measure it at room temperature using a Si sample with a known direct current (dc) conductivity.

No measurable microwave conductivity was detected in the temperature range below 20 K in the samples which showed no EDSR signal. Such samples were those not subjected to annealing or sample 6 which was annealed for a rather short time. In contrast, all the samples showing strong EDSR signals manifested remarkably high microwave conductivities even at 10 K with weak dependence on the temperature as will be shown later in Fig. 7. The value of  $\sigma_\omega$  was measured to be  $(1-5) \times 10^{-5} \text{ ohm}^{-1} \text{ cm}^{-1}$  at 10 K, while that of the dc conductivity  $\sigma_0$  at 10 K will always be lower than  $10^{-8} \text{ ohm}^{-1} \text{ cm}^{-1}$  with exponential dependence on temperature. A high microwave conductivity in CZ-Si annealed at  $650^\circ\text{C}$  was also reported in the previous works.<sup>13,14</sup>

In agreement with the previous work,<sup>14</sup> it was found that the band to band illumination leads to strong reductions in both microwave conductivity and EDSR signal in our samples. Figure 4 shows how the amplitude  $A$  of EDSR signal and the microwave conductivity  $\sigma_\omega$  at 10 K in sample 1 decrease with the increase in the intensity of illuminated light 1.2 eV in energy. The strong correlation between the EDSR intensity related to Si-SC1

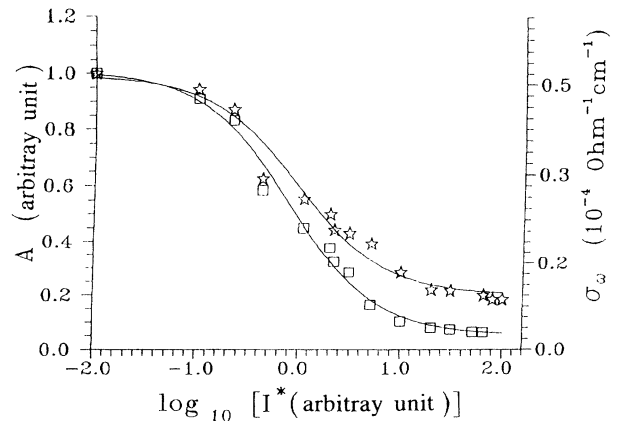


FIG. 4. Dependencies of the amplitude  $A$  of EDSR line shown by squares and microwave conductivity  $\sigma_\omega$  shown by stars in sample 1 on the intensity  $I^*$  of illumination light with a photon energy of 1.2 eV at 10 K.

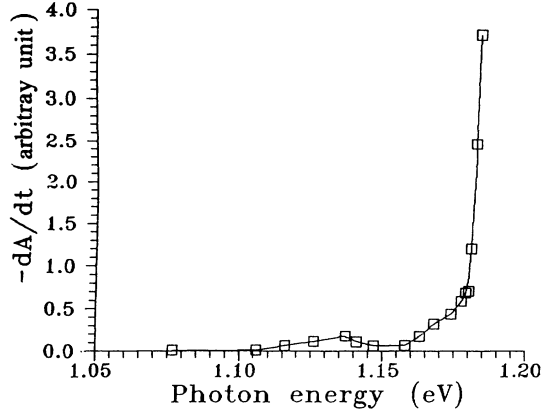


FIG. 5. Spectral dependence of the decreasing rate  $dA/dt$  of the EDSR signal amplitude at the onset of external illumination in sample 1 at 10 K. The data are normalized with respect to the number of incident photons.

centers and the microwave conductivity is clearly seen in the figure.

Figure 5 shows the spectral dependence of  $(dA/dt)_{t=0}$  in sample 1, where  $t$  is the time elapsed from the moment the light was turned on. The data are normalized with respect to the number of incident photons. It reflects the spectral dependence of the probability for the optical transition causing the decrease of the EDSR intensity.

#### D. Temperature dependence and saturation behavior of the EDSR

Figure 6 shows the dependencies of the amplitude  $A$  and the line width  $\Delta H$  of the EDSR line on the microwave power  $P \propto E_\omega^2$  for samples 1 and 2. The curves in the figure are in agreement with theoretical dependencies given by

$$A = A_0(1 + \beta E_\omega^2), \quad (3)$$

and

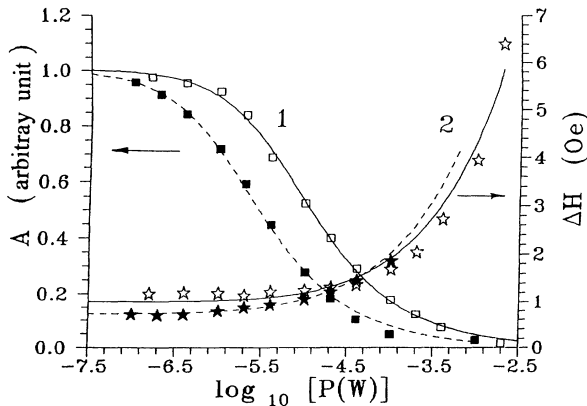


FIG. 6. Dependencies of the amplitude  $A$  and the width  $\Delta H$  of EDSR line on the microwave power  $P$  at 10 K. Open marks are for sample 1 and filled marks are for sample 2.

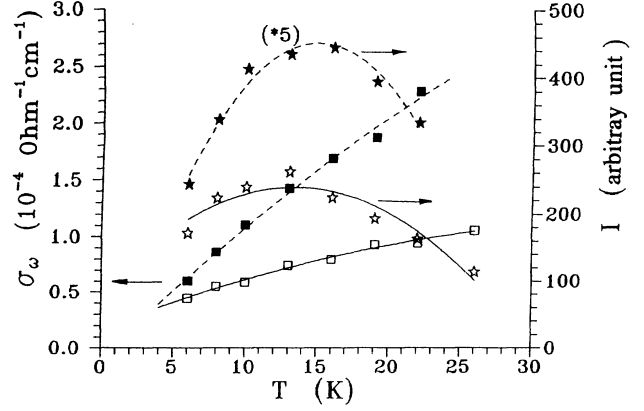


FIG. 7. Dependencies of EDSR intensity  $I (= A_0 T \Delta H^2)$  and the microwave conductivity  $\sigma_\omega$  on the temperature  $T$ . Open marks are for sample 1 and filled marks are for sample 2.

$$\Delta H = \Delta H_G + \Delta H_L(1 + \beta E_\omega^2)^{1/2}, \quad (4)$$

where  $\Delta H_G$  and  $\Delta H_L$  are the nonuniform and uniform contributions to the line width, respectively.  $\beta$  is equal to  $\gamma^2 \tau_1 \tau_2 \hbar^2 / E_\omega^2$ , where  $\gamma$  is the gyromagnetic ratio,  $\tau_1$  and  $\tau_2$  are the spin lattice and spin-spin relaxation times, respectively, and  $\gamma \tau_2 = 1 / \Delta H_L$ .  $\Delta H_G$  is 0.6–0.7 Oe and  $\Delta H_L$  is about 0.2 Oe at 10 K.

Figure 7 shows the dependencies of the EDSR line intensity  $I (\equiv A_0 \cdot T \cdot \Delta H^2)$  and the microwave conductivity  $\sigma_\omega$  on temperature. To avoid the effect of saturation and to improve the accuracy, we measured the saturation curves similar to that shown in Fig. 6 at each temperature and obtained the magnitude of  $I$  by extrapolating the curves to zero power.

## IV. DISCUSSION

### A. Origin of EDSR and microwave conductivity

Obviously, high microwave conductivity observed in our samples can be interpreted in terms of the conductivity along some extended defects which are visible by TEM observations. A good correlation between the EDSR intensity and the microwave conductivity leads us to the idea that the same kind of defects gives rise to both the microwave conductivity and the EDSR observed in our samples, since  $\sigma_\omega \propto N_r \cdot \text{Re}(\eta E_\omega) / E_\omega$  and  $I \propto N_r \cdot (\mathbf{V} \eta E_\omega)^2 / E_\omega$ , where  $N_r$  is the number of electrons participating in EDSR. The angular dependence of the EDSR line intensity strongly suggests that the concerned defects are quasi-one-dimensional defects lying along the  $\langle 110 \rangle$  directions. From TEM micrographs in Fig. 1 it is certainly plausible that the EDSR signals arise from electrons bound to the rodlike defects (RLD's) and/or dislocation dipoles (DD's). In the following we see whether all the results deduced from the analyses of the experimental data based on the above idea are consistent to each other or not.

First, we obtain the conclusion that the EDSR signal related to Si-SC1 centers are caused by RLD's and/or

DD's, which have trapped excess electrons from some shallow levels but not by RLD's and/or DD's in neutral state on the basis of the following facts.

(1) Under no illumination of light the EDSR signal is observed only in samples which are  $n$  type after thermal treatment. We have confirmed that a sample of CZ-Si heavily doped with boron at a concentration of  $5 \times 10^{15}$  atoms/cm<sup>3</sup> remains to be of  $p$  type after thermal treatment and shows no EDSR signal related to Si-SC1 under no illumination of light, despite that it contains RLD's and DD's at densities approximately the same as those in other samples shown in Table I. The microwave conductivity at low temperature has also been confirmed to be absent in such a sample.

(2) Optical band to band excitation causes a strong reduction in the EDSR signal intensity in  $n$ -type samples as has been shown in Figs. 4 and 5. Contrarily, the EDSR signal related to Si-SC1 has been detected in the  $p$ -type sample under the illumination which causes the band to band excitation.

These facts are interpreted in the following way. When extra electrons are trapped on Si-SC1 centers (which are RLD's or DD's) with the line density  $n_l$ , the Coulomb interaction causes band bending of the amount of

$$e\Phi \approx 2e^2 n_l [\ln(\lambda n_l) - 0.4] / \epsilon, \quad (5)$$

where  $\lambda$  is the screening radius and is equal to  $(n_l / \pi N_d)^{-1/2}$ , where  $N_d$  is the concentration of shallow donors being about  $10^{15}$  cm<sup>-3</sup> in the present case. In the  $n$ -type sample, in which Si-SC1 centers are negatively charged, the effective cross section for capturing extra electrons is smaller than that for holes approximately by a factor of  $\exp(e\Phi / k_B T)$ . Therefore, holes generated in the valence band under light illumination are captured by Si-SC1 centers much more effectively than electrons and lead to a decrease in  $n_l$ , while electrons are mainly trapped by ionized shallow donors. Hence, the curve in Fig. 5 reflects the optical cross section for generation of holes. The subsidiary peak seen at about 50 meV below the band gap energy may be related to the electronic states split from the valence band due to the stress field in the vicinity of Si-SC1 centers. In principle, it can also be related to the optical transition from the valence band to the ionized shallow donor states. Contrary to an  $n$ -type Si sample, electrons generated by light can be captured by Si-SC1 centers in a  $p$ -type sample and makes them slightly negatively charged. This is thought to result in the appearance of the weak signal of Si-SC1 EDSR which has actually been observed.

The appearance of high microwave conductivity means that the localization length  $L$  of electrons along a Si-SC1 center is sufficiently large to use formulas for microwave conductance  $\sigma_\omega$  which were deduced in a previous paper:<sup>11</sup>

$$\sigma_\omega = \text{Re} \{ e N_r \mu S(L/L_D) - i \Omega N_r [\mu m_e^* V S(L/L_D)]^2 R(\omega) / 8 k_B T \}, \quad (6)$$

where  $\mu$  is the mobility of electrons with microwave frequency  $\omega$  and  $m_e^*$  is the effective mass of electrons, both

along a Si-SC1 center.  $S(x)$  is a structural factor given by

$$S(x) = 1 - \exp(i\pi/4) \cdot \tanh[x \cdot \exp(-i\pi/4)] / x, \quad (7)$$

and  $L_D \approx [e\mu n_l \cdot \ln(L^2/b^2) / \epsilon\omega]^{1/2}$ , where  $b$  is the radius of the electronic wave function perpendicular to the center, being 0.5–3 nm, and  $\epsilon$  is the dielectric constant of Si.  $N_r$  in Eq. (6) is the number of electrons trapped on Si-SC1 centers whose density is  $N_{SC1}$ .  $N_r$  is related to  $N_{SC1}$  by  $N_r = N_{SC1} n_l$ .  $R(\omega)$  is the resonance function. In the case of a uniform line,  $R(\omega) = \Omega / (\omega - \Omega + i/\tau_2)$ , where  $\Omega$  is the spin resonance frequency  $\Omega = g\mu_B H_0 / \hbar$ . The nonresonant microwave conductivity we measured is related to the real part of the first term in Eq. (6). Thus,  $\sigma_\omega = e N_r \mu \cdot \text{Re}[S(L/L_D)]$ . The absorption intensity of the EDSR line corresponds to the real part of the second term of Eq. (6). Since  $S(L/L_D)$  is a complex function, the shape of an EDSR line is related to the mixture of the real and imaginary parts of  $R(\omega)$  (see Fig. 2).

## B. Estimation of parameter values

We are now able to estimate the magnitudes of some parameters associated with Si-SC1 centers from the shape of the EDSR line. By means of fitting experimentally obtained EDSR spectra to the theoretical curves we determined the values of  $L/L_D$  and  $I_0 = N_r \mu^2 V^2$ . The star marks in Fig. 8 show the values of  $L/L_D$  as a function of temperature. In the temperature range lower than 25 K,  $V$  does not depend on  $T$ . Therefore, dividing  $I(T)$  by  $\sigma_\omega(T)$  and taking into account the dependence of  $L/L_D$  on  $T$ , we obtain the dependence of  $\mu$  on  $T$ . The results are shown in Fig. 9. The dependence is well approximated by  $\mu \sim T^{-1}$ . Similarly, dividing  $\sigma_\omega^2(T)$  by  $I(T)$ , we obtain  $N_r$  as a function of  $T$ , which is shown in Fig. 8.

Discussion up to here gives the values of quantities in arbitrary units. To obtain the absolute magnitudes, we have to determine the magnitude of, at least, one of these quantities. We estimate roughly the number of trapped electrons  $N_r$ . If the energy level of Si-SC1 centers is  $E_r$ ,

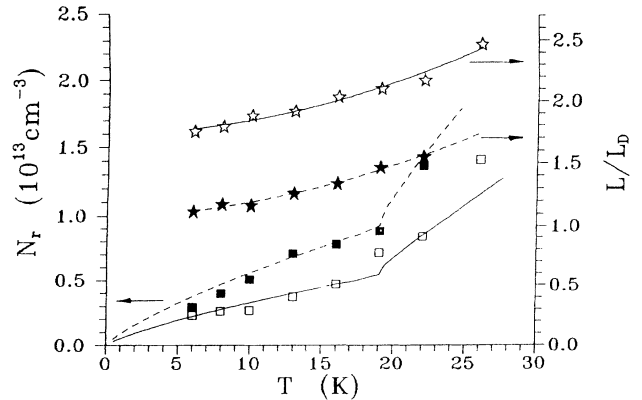


FIG. 8. Dependencies of the number of trapped electrons  $N_r$  and the localization length  $L/L_D$  of Si-SC1 on the temperature  $T$ . Open marks are for sample 1 and filled marks are for sample 2.

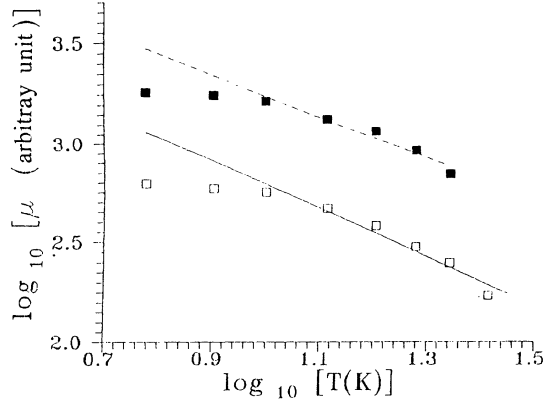


FIG. 9. Dependencies of the electron mobility  $\mu$  at microwave frequency on the temperature  $T$ . Open marks are for sample 1 and filled marks are for sample 2.

then in thermal equilibrium we have

$$e\Phi \approx E_F - E_r + k_B T \ln(an_t), \quad (8)$$

where  $E_F$  is the Fermi level ( $E_F \approx E_C - 0.04$  eV),  $1/a$  is the linear density of states on a Si-SC1 center. With the assumption  $E_r = E_C - 0.2$  eV, the magnitude of  $1/n_t$  turns out to be about 5 nm from Eq. (5). Taking into account the observations that the experimental density of RLD's or DD's is about  $2 \times 10^7$  cm $^{-2}$ , we obtain  $N_r$  to be about  $4 \times 10^{13}$  cm $^{-3}$ .

Actually, in a standard Oxford EPR cryostat used in our experiment, the sample placed in a quartz tube was not in thermal equilibrium, but always subjected to intensive room temperature infrared radiation coming from the wall of the microwave cavity. It excites electrons from both Si-SC1 centers and shallow donors to the conduction band with some probabilities  $G_r$  and  $G_d$ , respectively, and decreases the magnitude of  $n_t$  from that in thermal equilibrium. At low temperatures  $G_r$  and  $G_d$  are much higher than those of thermal activation. In such a case  $e\Phi$  is given by

$$e\Phi = k_B T [\ln(s_d/s_r) + \ln(G_d/G_r) - \ln(n_t a) - \ln\xi], \quad (9)$$

where  $s_r$  and  $s_d$  are the capture cross sections for Si-SC1 centers and shallow donors, respectively,  $\xi$  is the ratio of concentration of ionized shallow donors to the total donor concentration, and  $N_d$  is the total donor concentration.  $e\Phi$  is calculated by using Eq. (5).

Using the values of  $s_d/s_r$ ,  $G_d/G_r$ ,  $a$ , and  $\xi$ , which are thought to be appropriate for our experiments, we obtain  $1/n_t \sim 80$  nm and  $N_r \sim 2 \times 10^{12}$  cm $^{-3}$  at 10 K. In the low-temperature range  $n_t$  is proportional to  $T$ , while at temperatures higher than 20 K the rate of thermal activation for shallow donors becomes high and, as a consequence,  $n_t$  increase much faster with the increase in temperature.  $N_r$  versus  $T$  relations calculated with Eq. (9) are shown by lines in Fig. 8. From the above discussion we may conclude that the magnitude of  $N_r$  is of the order of  $10^{12} \sim 10^{13}$  cm $^{-3}$ .

To have the experimentally obtained magnitude of  $\sigma_\omega$ , the mobility  $\mu$  of electrons along a Si-SC1 center should be of the order of 100–1000 cm $^2$ /V s. It means that the localization length  $L$  must be 80–200 nm.

Comparing the EDSR signal intensity of sample 1 with the EPR signal intensity of Mn standard, we found that the EDSR absorption of the former is equivalent to the EPR of  $3 \times 10^{16}$  spins/cm $^3$ . Therefore, the *amplification factor*  $K = h_\omega^2/H_\omega^2$  turns out to be  $3 \times 10^{16}/N_r \sim 10^4$ . From the saturation data in Fig. 6 we have  $\tau_2 = 1/\gamma\Delta H_L = 3 \times 10^{-7}$  s. On the one hand, since  $\alpha = \gamma^2\tau_1\tau_2 K = 2 \times 10^5$ , we obtain  $\tau_1/\tau_2 \approx 10^{-13}$  s $^2$ . It means  $\tau_1 \approx \tau_2 \approx 3 \times 10^{-7}$  s.

### C. Identification of Si-SC1 center

The decrease of  $\mu$  with increasing temperature and a rather large localization length  $L$  of the order of 100 nm imply that the microwave conductivity and EDSR observed in the heat-treated CZ-Si may reasonably be attributed to some one-dimensional energy band. As can be seen in Fig. 1(c), RLD's are always observed to be very straight and their lengths are measured to be longer than 1  $\mu$ m even in sample 1. Therefore, the localization length of the order of 100 nm seems not to be unreasonable for RLS's. Contrarily, dislocations constituting DD's are often observed to be curved. It is not clear from TEM observations whether the electron localization length  $L$  for DD's is as large as 100 nm or not.

It is interesting to compare the intensity of EDSR related to Si-SC1 centers with the data of TEM observations. The intensity of the signal at any given temperature depends not only on the number of the electrons  $N_r$  which participate in resonance, but also on  $\mu$ ,  $L$ , and  $V^2$ . The magnitudes of these quantities may be different among samples prepared in different ways. However, when the EDSR is strongly saturated under a high microwave power, the amplitude of EDSR does not depend on  $\mu$  or  $V$  but depends only on  $N_r/T\tau_1$ . Results of TEM observations and EDSR measurements are shown in Table I for samples subjected to different heat treatments. The EDSR intensities shown in Table I are those measured at 10 K under a high microwave power ( $\sim 1$  mW) and are proportional to  $N_r$ .

One can see from Eq. (9) that  $N_r$  depends not only on the density of the defects but also on the compensation rate of shallow donors  $\xi$ . Table I shows that  $\xi$  assumes approximately the same values in samples 3–6, all of which are doped with boron. Thus, we compare the EDSR intensity with the density of the defects observed by TEM with these samples. We see that the EDSR intensity has a better correlation with the density of RLD's than the density of DD's.

The authors of the previous work<sup>14</sup> *a priori* assumed that EDSR-active centers found in heat-treated CZ-Si are DD's. They insisted that such assumption was justified by their results that the second axis of the  $g$  tensor was approximately parallel to the  $\langle 113 \rangle$  directions which was specific for dislocation dipoles. However, their reasoning seems not very clear. The  $g$  tensors determined in the present work do not coincide with those reported in the

previous work.<sup>14</sup> Thus, we suppose that Si-SC1 centers are not identical to Si-2K to Si-4K centers termed in the previous work. However, since the exact  $g$ -tensor parameters are found to depend on the thermal history of samples to some extent, we cannot exclude completely the possibility that centers found in the two works are identical to each other.

It is emphasized here that the  $\langle 113 \rangle$  directions are specific for the geometry of the RLD rather than the DD. TEM observations have revealed that the RLD's usually assume the shape of  $Z$  or  $V$  within the plane perpendicular to their long direction. In the case of the RLD parallel to the  $[110]$  direction it has wings lying on the  $(\bar{1}\bar{1}3)$ ,  $(001)$ , and  $(\bar{1}13)$  planes.<sup>6,7</sup> This picture agrees well with our EDSR data. With such a geometry the RLD should have the main axis  $L$  of the  $g$  tensor parallel to the  $[110]$  direction and the second axis  $Y$  in the direction somewhere between the  $[1\bar{1}3]$  and  $[001]$  or between the  $[\bar{1}13]$  and  $[001]$ , in quite good agreement with our experimental observations. We believe that the  $Y$  axis coincides with the direction of  $V$ , the direction along which the inversion symmetry is lost. The  $g$  factor must be most strongly deviated from the  $g$  value of free electrons along this direction in agreement with our observation.

## V. CONCLUSION

A series of EDSR lines, termed Si-SC1 in this paper, have been found to develop in CZ-Si due to annealing at 650°C. Some of these lines are very close to Si-2K and Si-3K reported in an earlier paper.<sup>14</sup> It has been shown that the experimental data are self-consistently interpreted with the model that Si-SC1 is related to excess electrons trapped by long quasi-one-dimensional defects lying along the  $\langle 110 \rangle$  directions. The localization length  $L$  of such electrons along the defect is rather long and has been estimated to be of the order of 100 nm. The electron mobility along the defect has been determined to be rather high, being higher than or about 500 cm<sup>2</sup>/Vs at 10 K. It decreases with increasing temperature.

TEM observations have verified that two kinds of extended dislocations are developed along the  $\langle 110 \rangle$  directions; namely, rodlike defects and dislocation dipoles. Thus, we have been led to the conclusion that relatively a deep quasi-one-dimensional energy band is associated with the regular straight parts of such defects. The analysis of the EDSR data suggests that it is better supported by an assignment to the rodlike defects than to the dislocation dipoles.

\*On leave from Institute of Solid State Physics, Russian Academy of Sciences, Chernogolovka, Russia.

†On leave from Institute of Electron Technology, Warsaw, Poland.

<sup>1</sup>A. Bourret, J. Thibault-Desseaux, and D. N. Seidman, *J. Appl. Phys.* **55**, 825 (1984).

<sup>2</sup>M. Reiche and O. Breitenstein, *Phys. Status Solidi A* **101**, K97 (1987).

<sup>3</sup>H. Bender, *Phys. Status Solidi A* **86**, 245 (1984).

<sup>4</sup>R. C. Newman, *J. Phys. C* **18**, L967 (1985).

<sup>5</sup>M. Reiche, J. Reichel, and W. Nitzsche, *Phys. Status Solidi A* **107**, 851 (1988).

<sup>6</sup>A. Bourret, in *Microscopy of Semiconducting Materials, 1987*, edited by A. G. Cullis and P. D. Augustus, IOP Conf. Proc. No. 87 (Institute of Physics, London, 1987), p. 39.

<sup>7</sup>H. Bender and J. Vanhellemont, *Phys. Status Solidi A* **107**, 455 (1988).

<sup>8</sup>A. Kanamori and M. Kanamori, *J. Appl. Phys.* **50**, 8095 (1979).

<sup>9</sup>Y. Kamiura, F. Hashimoto, and M. Yoneta, *J. Appl. Phys.* **65**, 600 (1989).

<sup>10</sup>Y. Kamiura, F. Hashimoto, and M. Yoneta, *J. Appl. Phys.* **68**,

1358 (1990).

<sup>11</sup>V. V. Kveder, A. E. Koshelev, T. R. Mchedlidze, Yu. A. Ossipyan, and A. I. Shalynin, *Zh. Eksp. Teor. Fiz.* **95**, 183 (1989) [*Sov. Phys. JETP* **68**, 104 (1989)].

<sup>12</sup>M. Wattenbach, C. Kisielowski, H. Alexander, V. V. Kveder, T. R. Mchedlidze, and Yu. A. Ossipyan, *Phys. Status Solidi B* **158**, K49 (1990).

<sup>13</sup>V. M. Babich, H. P. Baran, A. A. Bugai, A. A. Konchits, and V. M. Maksimenko, *Pis'ma Zh. Eksp. Teor. Fiz.* **44**, 513 (1986) [*JETP Lett.* **44**, 660 (1986)].

<sup>14</sup>V. M. Babich, N. P. Baran, A. A. Bugai, A. A. Konchits, and B. D. Shanina, *Zh. Eksp. Teor. Fiz.* **94**, 319 (1988) [*Sov. Phys. JETP* **67**, 1697 (1988)].

<sup>15</sup>E. I. Rashba, *Usp. Fiz. Nauk* **84**, 557 (1964) [*Sov. Phys. Usp.* **7**, 823 (1964)].

<sup>16</sup>T. Iizuka, S. Yakasu, M. Tajima, T. Arai, T. Nozaki, N. Inoue, and M. Watanabe, *J. Electrochem. Soc.* **132**, 1707 (1985).

<sup>17</sup>M. Suezawa, K. Sumino, and M. Iwaizumi, *J. Appl. Phys.* **54**, 6594 (1983).

<sup>18</sup>R. Worner and O. F. Schirmer, *Phys. Rev. B* **34**, 1381 (1986).

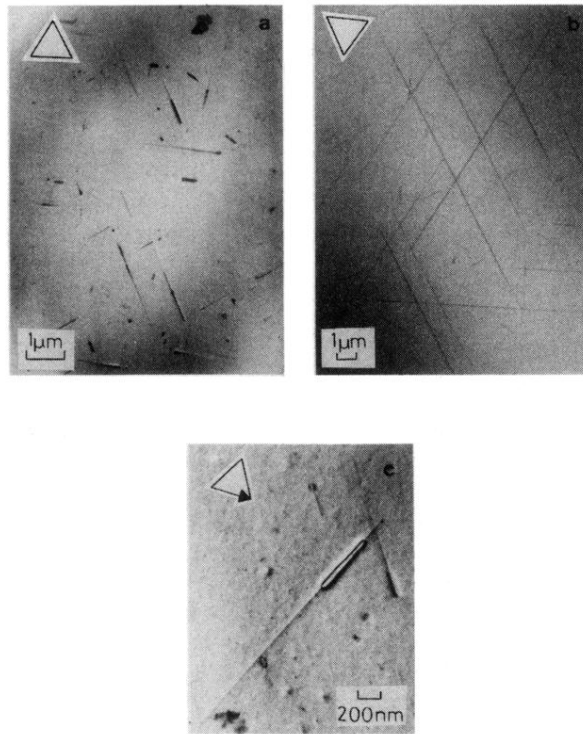


FIG. 1. Transmission electron micrographs of (a) sample 1, (b) sample 2 under the multibeam condition, and (c) sample 1 under the two-beam condition with diffraction vector  $\bar{2}20$ . Triangles shown on the micrographs consist of lines parallel to the  $\langle 110 \rangle$  directions lying on the film plane.